Invited Paper

Journal of Nonlinear Optical Physics & Materials
Vol. 8, No. 2 (1999) 191–210

OPTICAL NONLINEARITIES OF METAL-DIELECTRIC COMPOSITES

N. N. LEPESHKIN, W. KIM, V. P. SAFONOV*, J. G. ZHU, R. L. ARMSTRONG, C. W. WHITE†, R. A. ZUHR† and V. M. SHALAEV
Department of Physics, New Mexico State University, Las Cruces, NM 88003, USA

Received 16 March 1999

Nonlinear optical properties of metal-dielectric composites, such as fractal colloid aggregates and clusters created by ion implantation, are studied. Strong fluctuations of local fields result in huge enhancements of optical nonlinearities in fractal colloid aggregates. The real and imaginary parts of the cubic susceptibility of silver colloid aggregates are measured. It is found that the coefficient of nonlinear absorption strongly depends on the laser wavelength and intensity. Optical limiting effect in fractal silver colloids is observed. Nondegenerate forward four-wave mixing technique is used to investigate the third-order nonlinear susceptibility for nanocomposite material with Au nanocrystals formed inside a SiO_2 glass matrix. The Au nanocrystals are formed by the ion implantation and annealing method that produces very high volume fraction of nanoparticles. The large value $|\chi^{(3)}| = 1.3 \times 10^{-7}$ esu is measured. Two characteristic relaxation times, 5.3 ps and 0.66 ps, are estimated from the detuning curve of $|\chi^{(3)}|$, as the probe beam wavelength changes. A novel class of optical materials, microcavities doped with nanostructured fractal aggregates, is also studied. In our experiments, lasing at extremely low pump intensities, below 1 mW, and dramatically enhanced Raman scattering was observed in microcavity/fractal composites.

1. Introduction

The physics of metal-dielectric composites has recently gained increasing interest because of their unique linear and nonlinear optical properties, and their high application potential as nonlinear media and media for optical data storage. There are two types of composites commonly used: spatially separated metal nanoparticles embedded in a dielectric host and fractal aggregates of metal nanoparticles formed, for example, in colloidal solutions.

Enhanced optical processes in composite structures were studied by Sipe, Boyd, and their co-workers both theoretically and experimentally.[1] The large nonlinear optical susceptibility, $\chi^{(3)}$, was reported for nanocomposites with gold,[2–6] silver,[2,3,7,8] copper,[8,9] and tin[10] particles. The high values of the susceptibility ($\chi^{(3)} \sim 10^{-6}$ esu)

*Also at Institute of Automation and Electrometry, Novosibirsk 630090, Russia.
†Also at Oak Ridge National Laboratory, Solid State Division, Oak Ridge, TN 37831, USA.

are caused by strong enhancement of the local fields in metal particles at the surface plasmon resonance and by the high hyper-polarizabilities of metal particles.[3] The third-order polarizabilities of small metal particles can reach as high values as those of resonant atoms, and moreover, metal particles possess much wider spectral band of resonances than atoms. The mechanisms contributing to the third-order polarizability of the nanoparticles were considered in previous reports,[3] including the saturation of the absorption by the electron gas inside the particle,[6,11] the saturation of the interband transition,[6] and the hot electron contribution.[6] Hot electron contribution ("Fermi smearing") for gold nanoparticles at $\lambda = 532$ nm for picosecond pulses was found to be the dominant one.[6] For a long pulse duration, heating of nanoparticle crystal lattice becomes essential.[12]

The response time of the cubic nonlinearity was measured by the pulse delay technique in degenerate four-wave mixing (DFWM) experiments.[3,4,6,8,9,13] It was found that there are fast and slow relaxation processes, and the fast decay time is shorter than the pulse duration, which was typically several picoseconds. The recent investigations of electron dynamics in metal films and nanoparticles by the pump–probe technique with femtosecond pulses revealed femto- and picosecond relaxation processes,[14–17] the characteristic times of those were found to be dependent on the electron and lattice temperatures.[14]

There are two ways to increase the susceptibility of nanocomposites; they are (a) to increase the volume fraction of metal particles in the sample (it has been shown that high concentrations of nanocrystals can be achieved by ion implantation of high doses[8–10,13,18]), and (b) to aggregate the nanoparticles to form fractals, which will increase the enhancement factor in the long-wavelength spectral range substantially.[7]

One of the most interesting examples of metal fractal cluster media are colloidal aggregates in solutions. The optical properties of silver and gold colloidal solutions containing fractal clusters have been studied in several papers.[2,19–21] Nonlinear optical phenomena experience enhancement by several orders of magnitude in solutions of aggregated particles relative to those consisting of spatially separated nanoparticles.[19] The enhancement is associated with strong fluctuations of local field in metal fractal clusters.[22]

Optical excitations of nanomaterials with fractal structure result in highly localized dipolar modes.[22,23] The localized modes of fractals cover a broad spectral range, from the visible to the far-infrared. In metal fractals, collective plasmon oscillations are strongly affected by the fractal morphology, leading to the existence of "hot" and "cold" spots (i.e., areas of high and low local fields). Local enhancements in the "hot spots" exceed the average surface enhancement by many orders of magnitude[24–26]; this is because the local peaks of the enhancement can be spatially separated by distances much larger than the peak sizes. The spatial distribution of these high-field regions are very sensitive to the frequency and polarization of the applied field.[23–26] The positions of the "hot spots" change chaotically but reproducibly with frequency and/or polarization. This is similar to speckle created by

laser light scattered from a rough surface with the important difference that the scale-size for fractal plasmons in the hot spots is in the nanometer range rather than in the micrometer range for photons.

For the special case of fractals formed by metal particles, the dipole eigenmodes span the visible and infra-red regions of the spectrum. Since the mode quality-factors increase with the wavelength, the local fields are especially large in the long wavelength part of the spectrum. Calculations and experiments reveal a huge enhancement of the nonlinear responses in silver fractal clusters.[2,7,19,25] The enhancement factors for the Kerr nonlinearities grow considerably when the wavelength detunes from the monomer absorption peak, $\lambda = 400$ nm, toward the infrared.[25]

Enhancement of 10^6 times for a degenerate four-wave mixing in aggregated silver colloid in comparison with the non-aggregated was experimentally observed in Ref. 19. Frequency selective threshold photomodification of silver clusters was obtained when irradiating by nanosecond laser pulses with fluence $W \geq 1 \div 10$ mJ/cm^2.[19] Change in nonlinear response due to photomodification of silver colloid aggregates was also reported.[2,21]

This paper presents results of experimental studies of the four-wave mixing, nonlinear absorption and refraction of non-aggregated and aggregated metal nanocomposites. High-concentration non-aggregated Au-silica composite and aggregated colloids of Au and Ag nanoparticles are studied. It is shown that metal fractal structures possess very high optical nonlinearities. The figure of merit (FOM), $|\chi^{(3)}|/\alpha$, (where α is the linear absorption coefficient), and response time, which are important characteristics of a nonlinear medium, are measured and discussed. Sign reversal in the nonlinear absorption and refraction of aggregated metal colloid was observed when laser frequency and intensity changed. A novel class of optical materials, microcavities doped with fractal aggregates, is also studied. It is shown that fractal/microcavities composites possess unique optical properties, including extremely large linear and nonlinear susceptibilities.

2. Fractal Colloid Aggregates

In our experiments, colloidal solutions were prepared by two different techniques. In first method,[27] 1–3 mg of sodium boron hydrate was first dissolved in 20 ml of cooled distilled water (5 ml of water was used to dissolve silver nitrate). Then, the silver nitrate solution was quickly added to the test-tube with the sodium boronhydride solution and the mixture was intensively shaken. The resultant colloid was yellow-colored. After several days, the hydrosol aggregated and the solution color changed from yellow to green or grey. Gold colloids used in the experiments were prepared by similar techniques. In the second method of sample preparation,[28] 90 mg of $AgNO_3$ was dissolved in 500 ml of water and boiled. After that, 10 mL of 1% sodium citrate was added. The mixture was then boiled for 1 hour. In our experiments the aggregated silver colloid solution with the volume fraction filled by metal of 10^{-5} was used.

In Fig. 1, we show an electron microscope picture of a typical aggregate of silver colloidal particles. The fractal dimension for these aggregates is $D \simeq 1.7$. Note that voids are present in all scales from the minimum (about the size of a single particle) to the maximum (about the size of the whole cluster); this is an indication of the statistical self-similarity of a fractal cluster. The size of an individual Ag particle is approximately 10 nm, whereas the size of the whole fractal cluster is ~ 1 μm.

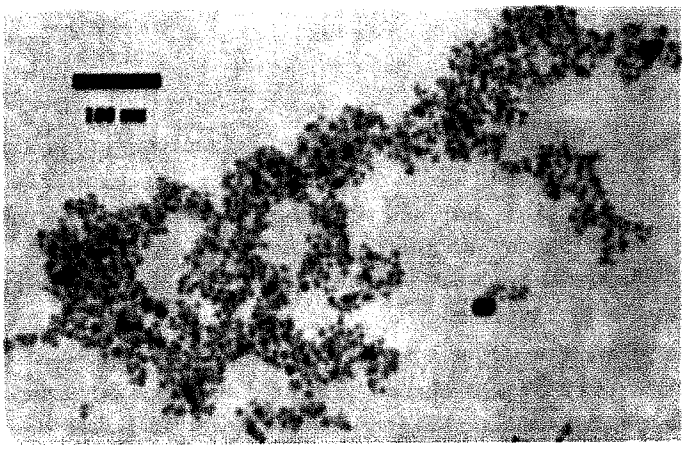

Fig. 1. Electron micrograph of a silver fractal cluster.

The absorption spectra for non-aggregated colloids exhibit a single peak related to the surface plasmon excitation at $\lambda \simeq 400$ nm for silver colloids, and at $\lambda \simeq 530$ nm for gold colloids. The absorption spectra for aggregated colloids are broadened in comparison to the non-aggregated. The broadening is caused by the interaction of dipoles induced by light in monomers, forming a cluster.

In our experiments we used an optical parametric oscillator MOPO 730 tunable within the range 440–700 nm with a pulse duration approximately 4 ns. The nanosecond pulses of Nd:YAG and Nd:$YAlO_3$ lasers at fundamental and second harmonic frequencies also were exploited. For the high intensity pulses we registered not only energy of the pulses, but also their temporal shape by using a Tektronix 2467B 400 MHz oscilloscope, a Tektronix C1002 videocamera, a Tektronix digitizing computer system DCS 01, and fast photodiodes.

The modulus of the cubic susceptibility of aggregated silver colloid was measured by degenerate four-wave mixing technique. The value of $|\chi^{(3)}| \simeq 10^{-9}$ esu was obtained for the most aggregated boron-hydride silver colloids with a volume fraction of metal, $p = 5 \times 10^{-6}$, at $\lambda = 1064$ nm for a laser intensity of 1 MW/cm^2.[2] This means that the susceptibility per unit volume of metal is more than 10^{-4} esu. The measured $|\chi^{(3)}|$ at $\lambda = 532$ nm is only one half of that. The figure of merit (FOM), $|\chi^{(3)}|/\alpha$, is about 10^{-9} esu $\cdot$ cm. The analogous spectral dependence was obtained for gold colloids.[29] The values of $|\chi^{(3)}|/p$ and FOM for aggregated colloid exceed

substantially (more than one to two orders of magnitude for nanosecond pulses) the corresponding values for non-aggregated composites at plasmon resonance[29] (see also below). The wavelength dependence of $|\chi^{(3)}|/p$ and FOM differ from those for non-aggregated samples significantly. Measurements with picosecond pulses show that the susceptibility is two orders of magnitude smaller than that with nanosecond pulses. This indicates that the thermal effects, namely heating crystal lattice[12] and host medium around absorbing particle, play essential role in the case of nanosecond pulses.

It is known that for certain optical switching and processing devices the refractive nonlinearity in the low absorption media is preferred. To measure the nonlinear refractive index, and the nonlinear absorption coefficient, we used the Z-scan technique.[30] This method allowed us to determine the nonlinear correction to the refractive index, n_2, and to the absorption coefficient, α_2, from experimental data and hence, calculate $\mathrm{Re}[\chi^{(3)}]$ and $\mathrm{Im}[\chi^{(3)}]$. It was found that for $\lambda = 540$ nm the aggregation of silver colloidal particles into fractal clusters was accompanied by the increase in nonlinear absorption from $\alpha_2 = -9 \times 10^{-10}$ cm/W to $\alpha_2 = -5 \times 10^{-7}$ cm/W, i.e., the enhancement factor was 560.[21] The enhancement factor exceeding 400 was obtained for the nonlinear refractive index. The calculated enhancement factors for the Kerr nonlinearity at $\lambda = 540$ nm are approximately 5×10^3. The values obtained for $\chi^{(3)}$ were $\mathrm{Re}[\chi^{(3)}] = 10 \times 10^{-11}$ esu, $\mathrm{Im}[\chi^{(3)}] = -8.3 \times 10^{-11}$ esu for $\lambda = 540$ nm, and $\mathrm{Re}[\chi^{(3)}] = -3.5 \times 10^{-11}$ esu, $\mathrm{Im}[\chi^{(3)}] = -2.7 \times 10^{-11}$ esu for $\lambda = 1079$ nm for $p = 5 \times 10^{-6}$. This suggests that the nonlinear absorption and the nonlinear refraction provide nearly equal contributions to the nonlinearity.

When the intensity exceeds 3 MW/cm^2, the results of the Z-scan fitting procedure from Ref. 30 become unsatisfactory. This implies that the nonlinearity deviates from the simple cubic law. To investigate the behavior at high intensities that significantly exceed the photomodification threshold, we used colloidal solutions prepared by the Lee and Meisel's method.[28] The concentration of the colloid solutions was adjusted so that $\alpha_0 = 1.6$ cm^{-1} at all wavelengths studied. The solution was placed in a cell with a thickness 10 mm and moved along a focused laser beam in order to vary the intensity of the incident pulse from approximately 1 MW/cm^2 to 318 MW/cm^2. The absorption coefficient was measured. Figure 2 summarizes our findings and presents the dependence of nonlinear correction to the absorption coefficient, $\Delta\alpha$, on the peak intensity of the incident radiation at $\lambda = 442$ nm, 532 nm, and 650 nm. The colloid displayed three different types of behavior for the absorption. At $\lambda = 440$ nm, the absorption of silver colloid dropped with the intensity, demonstrating the effect of nonlinear "bleaching." At $\lambda = 650$ nm, we observed the increasing absorption as a function of the intensity. At $\lambda = 532$ nm, the dependence of absorption on intensity was more complicated; it showed both nonlinear "bleaching" and darkening within certain intensity intervals. The analogous intensity dependence was observed at $\lambda = 1064$ nm.

Thus, we may conclude that both the absorption and the refraction nonlinearities of an aggregated silver colloid solution change their signs with the wavelength.

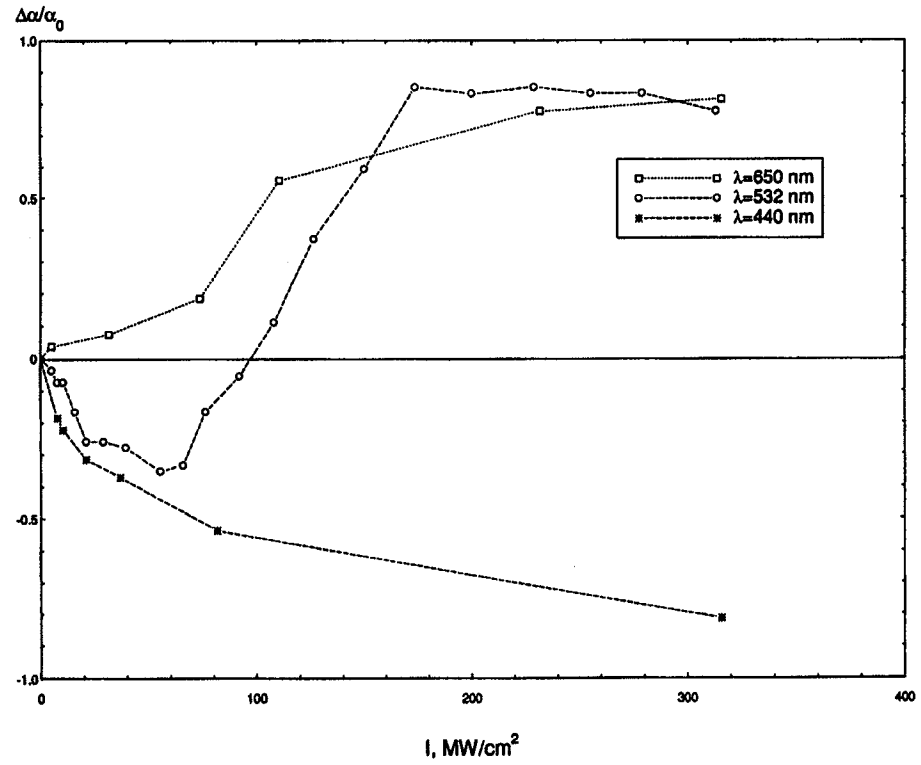

Fig. 2. Intensity dependence of the nonlinear correction to the absorption coefficient for different laser wavelengths at the peak of the incident pulse.

These changes may be related, on the one hand, to the variations of the signs of the enhancement factors.[25] On the other hand, and this is more likely, the sign changes may be due to the band structure of silver, laser heating of electron gas and crystal lattice of nanoparticles, and heating of the host medium surrounding the particles by thermal diffusion.

Two processes may be responsible for the darkening at high intensities: nonlinear absorption and nonlinear scattering. Actually, we observed the increase in scattering in an angular cone of width 0.05 rad when the darkening occurred, but the loss of laser energy due to the scattering was at least 10 times smaller than the absorbed energy. Backscattering and breakdown were not detected in our samples.

Figure 2 shows that the dependence $\Delta\alpha(I)$ at $\lambda = 440$ nm is similar to the saturated absorption curve under the conditions of photoburning of the resonant modes. When the intensity is relatively low, $I \leq I_{th} = 4$ MW/cm^2, the nonlinear absorption obeys the law $\Delta\alpha/\alpha_0 = (I/I_s)/(1+I/I_s) = (\alpha_2/\alpha_0)I$ with $\alpha_2 = -6.6 \times 10^{-8}$ cm/W; however, when the intensity exceeds the photomodification threshold, I_{th}, the photoburning of the resonance domains in colloid aggregates occurs, and the dependence of $\Delta\alpha(I)$ deviates from this law. The analogous behavior of nonlinear absorption was observed at $\lambda = 540$ nm for $I \leq 3.5$ MW/cm^2.[2,21]

The corresponding curve for higher intensities at $\lambda = 532$ nm in Fig. 2 shows that in the range 60–170 MW/cm^2 there is a linear increase of the absorption versus intensity. This suggests that, in this range, the main nonlinear absorption mechanism is two-photon absorption. The measured coefficient for two-photon absorption is $\alpha_2' = 1.7 \times 10^{-8}$ cm/W at the peak of the incident pulse ($\Delta\alpha = \alpha_2' \cdot I$). Approximately the same value of α_2' was obtained at $\lambda = 650$ nm for intensity $I \simeq 100$ MW/cm^2.

The temporal shape of laser pulses transmitted through the solution is given in Fig. 3 for different intensities. One can see from this figure that the contribution of two- (or multiphoton-) absorption increases during the laser pulse. This suggests that induced absorption is connected with heating or modification of silver nanocomposites by laser radiation.

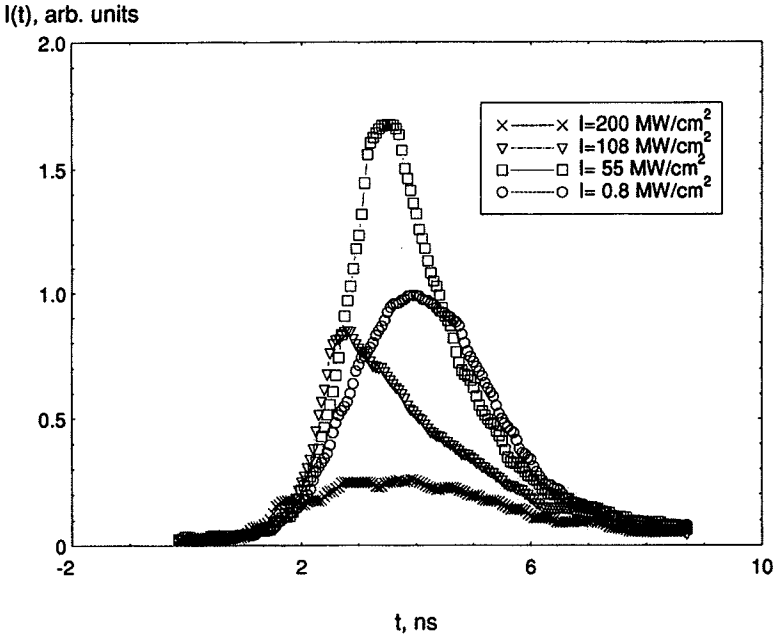

Fig. 3. Oscillograms of the laser pulses transmitted through the silver colloid for different incident intensities at $\lambda = 532$ nm.

This phenomenon may be interpreted as follows. The nonlinear optical "bleaching" is caused by the presence of aggregates of nanoparticles in solution leading to high local fields within fractal structures. Colloid aggregates are modified by high intensity light within $t \leq 10^{-9}$s, and the optical nonlinearity related to the fractal structure of the medium decreases.[19] After that, the weaker nonlinearity of isolated particles and bulk metal becomes essential. Therefore, 1 ns after the leading edge of the pulse, we observe the strong nonlinear absorption related probably to two-photon absorption in bulk silver. The above data shows that the coefficient of

two-photon absorption is 30 times smaller than that of nonlinear "bleaching" for low intensities. According to Ref. 31, the probability of two-photon absorption near the L-symmetry point increases with the wavelength as λ^8. That is why the effect of two-photon absorption is larger in the green region of the spectra than that in the blue region.

Increasing the intensity up to 100 MW/cm^2 leads to the optical limiting regime at $\lambda = 532$ nm, $\lambda = 650$ nm and 1064 nm (see Figs. 2 and 3); the energy of the transmitted pulse does not grow with increasing incident energy. Specifically, at the intensity $I \simeq 170$ MW/cm^2 at $\lambda = 532$ nm, the peak intensity of the transmitted pulse decreases to 1/5 of that in the linear absorption regime.

3. Non-Aggregated Gold Nanocomposites

Below, we consider nondegenerate four-wave mixing (FWM), $\omega_3 = 2\omega_1 - \omega_2$, in gold composites formed by ion implantation of SiO_2, where ω_1, ω_2, and ω_3 are the frequencies of the pump, probe, and signal waves respectively. The high value of $\chi^{(3)}(\omega_3) = (0.26 - 1.3) \times 10^{-7}$ esu was obtained in the range of the frequencies $|\omega_1 - \omega_2| \leq 28$ cm^{-1}.

The samples were prepared by implantation of Au^+ ions into Corning fused silica glass substrates. The implantation energy was 2.75 MeV with a dose of 1.5×10^{17} ions/cm^2. The substrate was heated during implantation and kept at 400°C to facilitate the formation of Au nanocrystals. The implanted Au concentration profile measured by Rutherford backscattering (RBS) is shown in Fig. 4. The thickness of Au^+-implanted layer is about 1 μm, the width at the 1/e peak concentration level is 0.65 μm. Cross-sectional transmission electron microscopy studies showed that the average diameter of gold particles in the samples was 6 nm.[32] At the center of the high concentration region, a few large Au particles have sizes almost 10 nm. At the low concentration regions, the small Au particles are about a few nanometers in sizes. The gold volume fraction p was estimated to be 7% in the implanted region. More details on the ion implantation of Au at different temperatures and doses can be found in Ref. 32.

The absorption spectrum of the samples measured with a HP spectrophotometer is shown in Fig. 5. The peak of the surface plasmon absorption is at $\lambda_p = 520$ nm and has a half-width at half-maximum $\Delta\omega_p = 2000$ cm^{-1}, which is close to the typical value for 6 nm Au particles.[19] The absorption in the short wavelength range is attributed to defect centers in SiO_2 induced by ion implantation. The near-infrared wing in the absorption spectrum can be attributed to collective effects resulting from the high concentration of Au particles.

The absolute value of the cubic susceptibility at the surface plasmon resonance of gold particles in silica is measured by a two-beam FWM configuration. The MOPO-730 is the source of the tunable probe wave, ω_2, with spectral width less than 0.2 cm^{-1}. The narrow-band pump wave, ω_1, is provided by the frequency-doubled output of a Nd:YAG laser. The pulse duration is 4 ns for the ω_2 beam

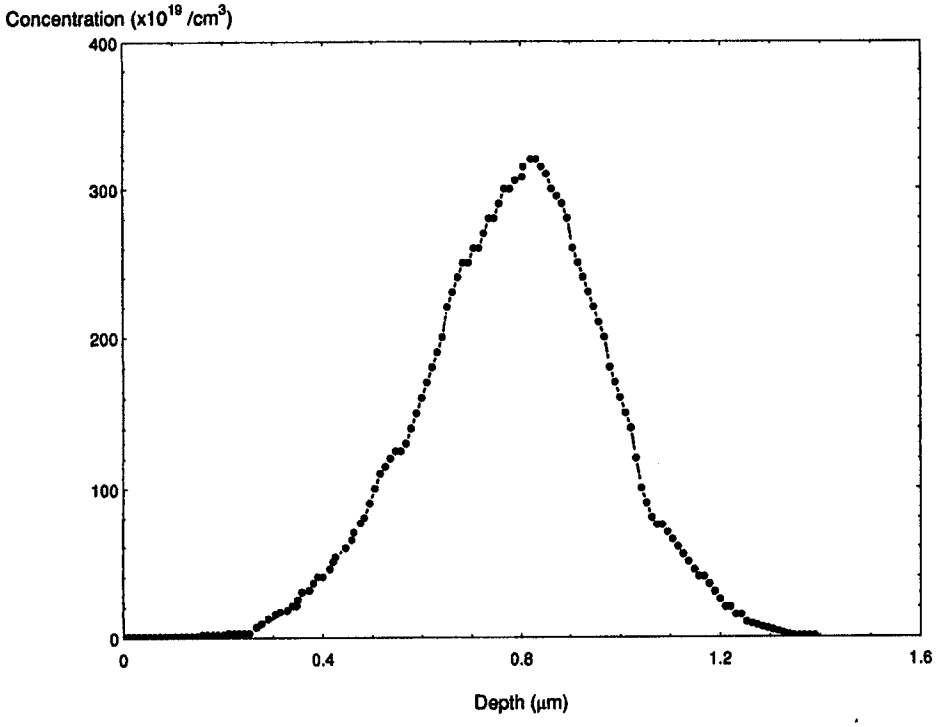

Fig. 4. Concentration profile of Au implanted into SiO_2 matrix measured by RBS.

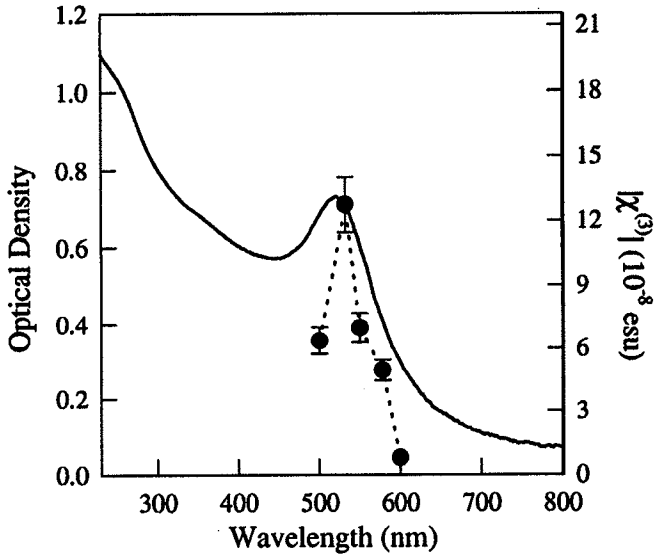

Fig. 5. Absorption spectrum (solid line) of the Au implanted glass sample and $|\chi^{(3)}|$ values (filled circles) measured by DFWM at different wavelengths.

and 10 ns for the ω_1 beam. The diameters of the beams are about 2 mm. Both beams have the same linear polarization. The intensity of the probe beam, I_2, is normally less than one half of the pump intensity, I_1. These two beams intersect in the sample at the relatively small angle (5°). The signal beam $\omega_3 = 2\omega_1 - \omega_2$ is emitted in the direction $\mathbf{k}_3$ symmetric to the probe wave vector, $\mathbf{k}_2$, with respect to the pump wave vector $\mathbf{k}_1$. A Tektronix 2467B oscilloscope, a C1002 video camera, a digital computer system DCS01, fast photodiodes, and neutral filters are used to measure the conversion efficiency for FWM, $\eta = I_3/I_2$, where I_3 is the intensity of the signal beam.

It is observed that $I_3 \propto I_1^2 I_2$ when the intensities of the incident beams I_1 and I_2 are less than 2 MW/cm^2. Taking into account that our medium is absorbing and that the frequency detuning range $|\omega_1 - \omega_2| \ll \Delta\omega_p$, we can calculate the absolute value of $\chi^{(3)}(\omega_3)$ from the following equation

$$\left|\chi^{(3)}(\omega_3)\right| = \frac{n^2 c \lambda_3}{24\pi^3} \times \frac{\alpha}{(1-T)\sqrt{T}} \times \frac{\sqrt{\eta}}{I_1},$$

where α is the absorption coefficient, $T = \exp(-\alpha l)$ is the transmittance, λ_3 is the wavelength of the signal, n is the refractive index, and c is the speed of light.[24] The values of α, T, and n are taken at the pump wavelength λ_1.

For DFWM at $\lambda_3 = \lambda_2 = 532.1$ nm and $I_1 = 1.9$ MW/cm^2, we have measured $|\chi^{(3)}| = 1.3 \times 10^{-7}$ esu. This value is several orders of magnitude larger than that measured for DFWM in the low-concentrated gold colloid solution[3] and gold-doped glass,[6] and it is also larger than that previously reported for ion implanted samples measured with picosecond pulses.[13] The corresponding susceptibility of gold particles $\chi_m^{(3)}$, which, according to Refs. 3 and 6, describes the nonlinear response to the internal field, is $\chi_m^{(3)} = \chi^{(3)}/(pf_1^2|f_1|^2) = 2.2 \times 10^{-7}$ esu, where p is the metal volume fraction and f_1 is the ratio between the internal field E_1 and external field E_0. For 6-nm particles, f_1 is estimated as 1.7.[6] Our value of $\chi_m^{(3)}$ is close to the value of 1.1×10^{-7} esu obtained in Ref. 6 for the nonlinear susceptibility due to the hot electron contribution. The $|\chi^{(3)}|$ values measured by the DFWM method at different wavelengths ($\omega = \omega_1 = \omega_2$) is shown in Fig. 5. Both the ω_1 and ω_2 waves were generated by the MOPO-730. The spectral width of DFWM $|\chi^{(3)}|$ as a function of ω is approximately one half of that of plasmon absorption peak. This means that the absorption is controlled by homogeneous broadening in our sample, and it can be explained by the effective medium theory.[10]

The $|\chi^{(3)}|$ values have also been measured by nondegenerate FWM by detuning the probe beam frequency ω_2. Figure 6 represents the dependence of $|\chi^{(3)}(\omega_3)|$ on the frequency detuning $|\omega_1 - \omega_2|$. The curves for $\omega_1 - \omega_2 > 0$ and $\omega_1 - \omega_2 < 0$ are almost symmetric. It is noteworthy that the value of $|\chi^{(3)}|$ decreases only by a factor of 5 for a detuning $|\omega_1 - \omega_2| = 28$ cm^{-1}. The dependence of $\chi^{(3)}(\omega_1 - \omega_2)$ changes slope in the log–log scale at $\Omega_a = |\omega_1 - \omega_2| = 1$ cm^{-1}, and at $\Omega_b = |\omega_1 - \omega_2| = 8$ cm^{-1}. At the first point the slope changes from 0 to 0.2, and at the second, from 0.2 to 1.

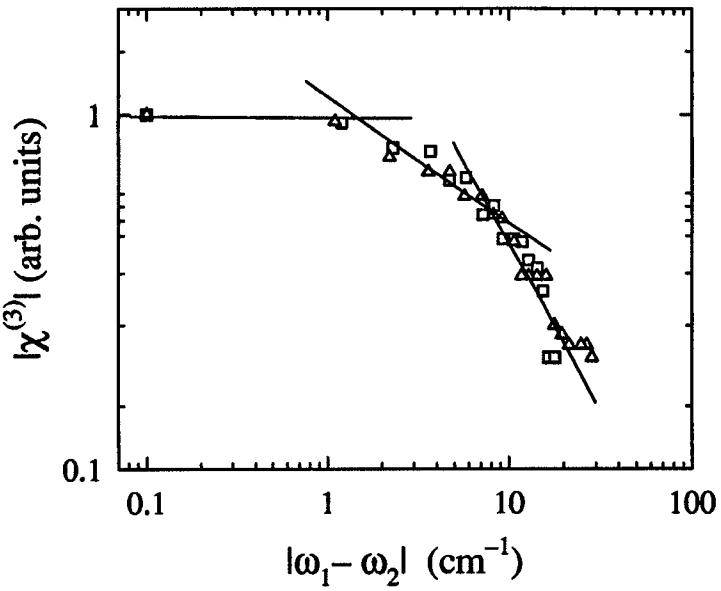

Fig. 6. Dependence of $|\chi^{(3)}|$ on the frequency detuning $|\omega_1 - \omega_2|$ (log–log plot). The square symbols represent data for $\omega_1 - \omega_2 > 0$, and triangular symbols for $\omega_1 - \omega_2 < 0$.

According to the simple model of FWM in a two-level system,[33] $\chi^{(3)}$ as a function of $|\omega_1 - \omega_2|$ may have two points of change of the slope on the curve mentioned above. These points correspond to longitudinal (τ_1) and transverse (τ_2) relaxation times. In this model, the slope at small $|\omega_1 - \omega_2|$ is 0; at intermediate detuning, the slope is 1; and, at large $|\omega_1 - \omega_2|$, the slope is 2.

To describe the $\chi^{(3)}$ dependence on ω_3 for a gold particle, a more complicated model was considered.[4] In Ref. 4 it is taken into account that plasmon oscillations decay nonradiatively into a reservoir of electron and phonon energy. This thermal reservoir cools down with relaxation time τ_v. The numerical analysis[4] showed that, for short τ_1 and τ_2 times, the lifetime associated with energy transfer into or out of the reservoir introduces another slope change to $\chi^{(3)}$. The $\chi^{(3)}$ dispersion calculated for $\tau_v = 5.3$ ps and $\tau_2 = 3.5$ fs showed slope changes at $|\omega_1 - \omega_2| = 1$ cm^{-1} and 1000 cm^{-1}.[4] The FWM signal at $2.8 < |\omega_1 - \omega_2| < 110$ cm^{-1} without the change of the slope was observed for gold particles with a diameter of 30 nm in colloidal solution.

We suppose that the points of the slope change in the detuning curve (Fig. 6) observed in our experiments correspond to characteristic times of the thermal diffusivity from a gold particle to a host medium, $\tau_v = \tau_a = (2\pi c\Omega_a)^{-1} = 5.3$ ps, and to electron-phonon energy relaxation time, $\tau_{ep} = \tau_b = (2\pi c\Omega_b)^{-1} = 0.66$ ps. The time of thermal diffusivity responsible for cooling a single-particle reservoir may be estimated as $\tau_v = c_1\rho_1 r^2/3\kappa_2 = 5.5$ ps (the values of gold lattice specific heat $c_1 = 0.13$ J/g·K, density $\rho_1 = 19.3$ g/cm^3 and silica thermal conductivity $\kappa_2 = 0.014$ W/cm·K were used). The evaluated lattice temperature of gold

nanoparticles in silica irradiated by a 2 MW/cm^2, 10 nanosecond pulse, $T_i = 350$°K, is approximately equal to the electron temperature. At the characteristic temperatures 300–600°K, for the thermally excited quasiparticles in the nonthermal electron model,[14] the electron–electron collision time is equal to the electron-phonon energy relaxation time, $\tau_{ep} = \gamma T_i/g = 0.77$ ps, where $\gamma = 66$ J/m^{3}K^2 (electron specific heat is $c_e = \gamma T_e$), and electron-phonon coupling coefficient $g = 3 \times 10^{16}$ W/m^3·K. One can see good agreement between the measured values τ_a, τ_b and the estimated τ_v, τ_{ep}.

For DFWM process, we note that the FOM value drops sharply with detuning of the laser frequency from the surface plasmon resonance. The FOM is 4.5×10^{-12} esu·cm at $\lambda = 532$ nm and 6.3×10^{-13} at 600 nm. Quite different spectral dependence is found for the aggregated gold colloid.[29] Aqueous gold colloidal solutions were prepared by the method.[34] The measured values are $\chi^{(3)} = 0.56 \times 10^{-10}$ esu at 532 nm and 2.4×10^{-10} esu at 1064 nm. The FOM also increases toward the infrared, with the value at 1064 nm of 1.7×10^{-10} esu·cm. These data show the increase in the local field enhancement in gold aggregates and it is in agreement with the data for silver aggregates discussed above.

To determine contributions of the real and imaginary parts to $\chi^{(3)}$, we have done the z-scan measurements (by the technique from Ref. 30) with gold colloids at $\lambda = 532$ nm. It was found that the imaginary part of the $\chi^{(3)}$ exceeds the real one, as expected.

4. Fractal Aggregate/Microcavity Composites

The giant enhancement of the optical response in fractal colloid metal aggregates has been analyzed in the preceding paragraphs. However, there exists an alternative approach for achieving large enhancement of optical responses which involves the exploitation of morphology-dependent resonances (MDR's) in dielectric microcavities.[35] These resonances, which have high quality factors ($Q = 10^5 - 10^9$), result from confinement of the radiation within the microcavity by total internal reflection.

Light emitted or scattered in the microcavity may couple to high-Q MDR's lying within its spectral bandwidth, leading to enhancement of both spontaneous and stimulated optical emissions. For example, enhanced fluorescence emission from an organic dye-doped cylindrical or spherical microcavity occurs when either the laser pump or the fluorescence (or both) couple to microcavity MDR's.[36] Moreover, the increased feedback produced by MDR's is sufficient to obtain laser emission from a dye-doped microdroplet under both cw[37] and pulsed[35] laser excitation, with a threshold cw pump intensity three orders of magnitude lower than that of a conventional dye laser in an external cavity.

The existence of high-Q microcavity modes is also responsible for stimulated nonlinear effects including:

(1) Stimulated Raman and Rayleigh-wing scattering and four-wave parametric oscillation under moderate intensity cw excitation[38];

(2) A large (> 100) quantum electrodynamic (QED) enhancement[35] arising from MDR-induced changes in the density of states; the largest enhancement occurs when the MDR mode spacing is greater than the homogeneous linewidth of the nonlinear process while the latter is greater than the MDR mode width;
(3) Optical bistability connected with the thermal nonlinearity of fused silica microspheres under low power (10^{-8} W) cw excitation.[39]

Although strong existing evidence suggests that fractal nanocomposites and microcavity resonators individually result in large enhancements of optical emissions, recent experiments performed in the laboratory of some of us[40] confirm that, in fractal aggregate/microcavity composite media, giant, multiplicative enhancement factors are obtained under the simultaneous, combined action of these two resonant processes when an emitting species is adsorbed onto metal fractal aggregates contained within high-Q microcavities. We observed lasing from Rhodamine 6G (R6G) dye molecules adsorbed onto silver colloidal aggregates seeded into a cylindrical microcavity for dye molarities approximately 3 orders of magnitude lower than for the corresponding microcavity dye laser in the absence of colloidal aggregates, and for a threshold pump intensity approximately 3 orders of magnitude less than for a conventional dye laser. The enhancement factor for Raman scattering resulting from fractal aggregate collective resonance modes was found to be 3×10^5, with an additional (multiplicative) enhancement factor greater than 1.5×10^4 due to MDR's of a silica microcylinder containing the fractal aggregate solution. We believe that these findings demonstrate the unique potential of such devices in the development of ultralow threshold microlasers, nonlinear-optical devices for photonics, as well as new opportunities of microanalysis.

Silver fractal aggregate colloid solutions, which were prepared using the method of (see Ref. 28), consist of silver monomers of average diameter 25 nm with aggregates typically containing 10^3 monomers. The absorption spectra of non-aggregated silver colloids exhibit the surface plasmon resonance feature at 400 nm, which, with aggregation, results in the appearance of a broad wing extending toward the long-wavelength part of the spectrum (see Fig. 7(c)).

In lasing experiments, a small amount of a parent solution of 10^{-4} M R6G dye in methanol was added to the colloid solution; the resulting dye concentration in the samples studied ranged from $10^{-8} - 10^{-5}$ M. A cylindrical microcavity was fabricated from a cylindrical quartz tube (inner and outer diameters, 0.7 and 1.0 mm), and the dye/colloid solution placed within the tube. A 10 mW cw Argon-ion laser (514.5 nm) and a 0.75 mW cw green He-Ne laser (543.5 nm) were used as pumping sources. The pump beam (approximately 2 mm in diameter) was focused into the tube by a 75 mm focal length lens; focal plane beam diameters were 70 μm and 35 μm for the Argon and HeNe lasers. Pump beam polarization was vertical (along the axis of the tube), and output radiation was collected at 90 degrees to the incident radiation as shown in Figs. 7(a) and 7(b). Spectroscopic measurements were performed using a CCD camera mounted to a SpectraPro-300i spectrograph; an 1800

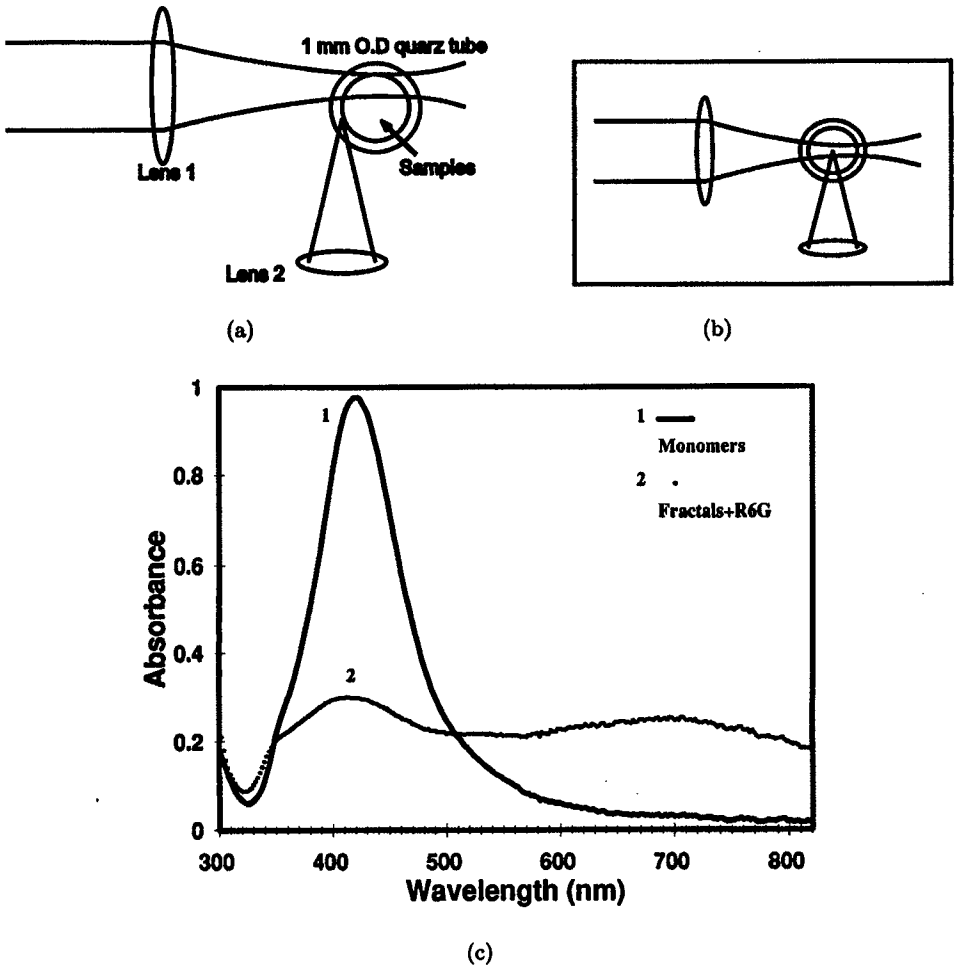

Fig. 7. Schematic diagram of the experimental configurations: (a) Microcavity MDR's efficiently excited; (b) MDRs effectively unexcited; (c) Absorption spectra of silver colloidal particles (1) and their fractal aggregates (2) in 1 mm path length cell. Lens 1, focal lengths 75 mm; lens 2 used for f/number matching into spectrograph. Quartz cylinder inner diameter, 0.7 mm.

groove per millimeter grating provided a full width at half maximum (FWHM) spectral resolution of 0.04 nm.

Elastic scattering of a laser beam passed through the outer edge of the empty cylindrical tube exhibited well-defined, MDR angular structure; when the beam was passed through the inner edge of an empty tube (see Fig. 7(a) — most of our experiments were performed using this illumination geometry), the MDR intensity significantly decreased. However, filling the tube with a colloidal solution again resulted in strong elastic scattering with a clearly resolved MDR angular structure; this observation suggests that light scattering by colloidal particles facilitates trapping of the radiation in the MDR's cavity modes. Alternatively, for some calibration

experiments, we did not wish to excite MDR; for these experiments, pumping scheme 7(b) was used.

Elastic scattering by fractal aggregates and monomers also contributes to outcoupling of radiation from microcavity MDR's. Scattering, together with absorption, decreases the Q of the cavity modes according to $Q^{-1} = Q_a^{-1} + Q_{SV}^{-1} + Q_{SS}^{-1}$, where Q_a^{-1}, Q_{SV}^{-1}, Q_{SS}^{-1} are losses due to absorption, volume scattering, and surface scattering.[35] (Diffraction losses are negligible in our case.) If colloidal aggregates are present in the microcavity, volume absorption is the most important loss mechanism. The measured absorption coefficient at 543.5 nm is $\simeq 5\ \text{cm}^{-1}$ yielding $Q_a \simeq 3.4 \times 10^4$. The measured scattering loss, Q_{SV}^{-1}, is smaller than Q_a^{-1} by at least an order or magnitude, implying that scattering may be regarded in our experiments simply as an outcoupling mechanism for microcavity radiation.

Figure 8 contrasts the luminescence spectrum of a 5×10^{-7} M dye solution in a microcavity with and without the presence of fractal aggregates. Without aggregates, under 514.5 nm excitation, a weak, broad luminescence band is observed with a maximum near 560 nm and a FWHM of 30 nm; the lower trace in Fig. 8 shows the central portion of this spectrum and the insert provides an expanded view. In the insert, representative groupings of small amplitude peaks may be seen corresponding to luminescence emission coupled to microcavity MDR's. The intermode spacing between these peaks is approximately 0.066 nm, which is slightly smaller than the theoretical intermode spacing, 0.078 nm, for a quartz cylinder of radius, $a = 0.5$ mm, and refractive index, $n = 1.46$. However, in our experiments, the effective path length of a single traversal of the cavity may be greater than $2\pi a$, because, multiple, near-field scattering in a colloidal solution plays an essential role in the coupling between molecular emissions and microcavity MDR's; the increased effective path length would result in the observed decrease in.

In the presence of dye-doped fractal aggregates, the luminescence intensity and spectrum are changed dramatically. Figure 8 illustrates the huge increase in MDR peak intensities in a narrow spectral region centered near 561 nm with a bandwidth of approximately 3 nm. The minimal spacing between peaks in this region is the same as for pure dye luminescence (i.e., in the absence of fractal aggregates). However, their spectral widths, limited by our instrumental resolution, are approximately 0.04 nm; this spectral width allows us to estimate a lower bound for the MDR $Q > 1.5 \times 10^4$.

Similar results were observed for the spectrum of a R6G-doped aggregated silver colloid solution in a microcavity excited by a 543.5 HeNe laser; huge MDR peaks are centered near 600 nm in this case. The narrowing of the emission spectrum (from 30 nm to 3 nm) is characteristic of laser action. To test this hypothesis, the emission intensity of different spectral components was studied as a function of pump intensity. It was found that this dependence is linear for low excitation intensities for all spectral components. However, when the pump intensity exceeded 20–50 W/cm^2, some peak signals grew strongly, exhibiting a lasing threshold

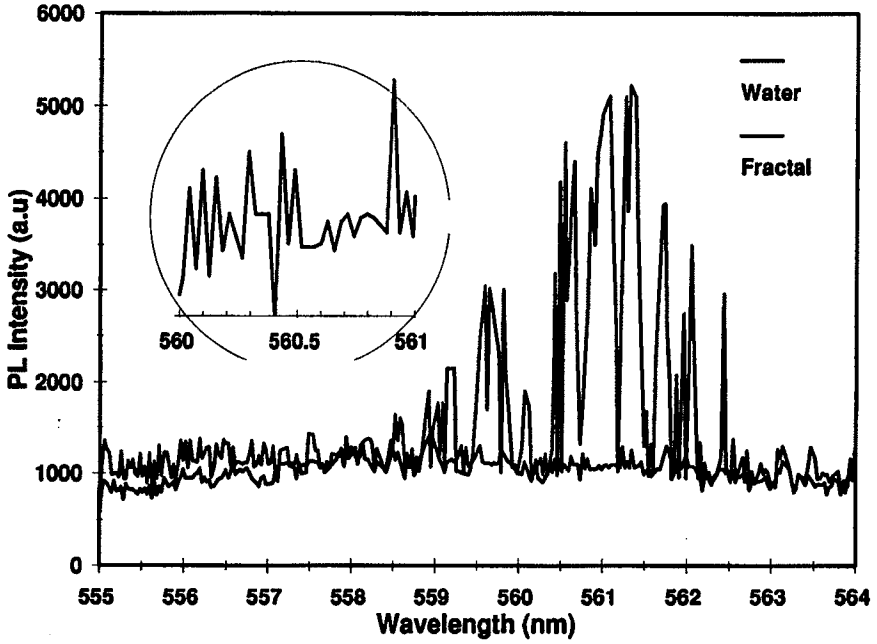

Fig. 8. Luminescence spectrum of 5×10^{-7} M R6G dye solution in microcavity, with (heavy line) and without (thin line) fractals, for $\lambda_L = 514.5$ nm, cw Argon laser excitation. Insert gives detail of spectrum without fractals showing typical mode structure.

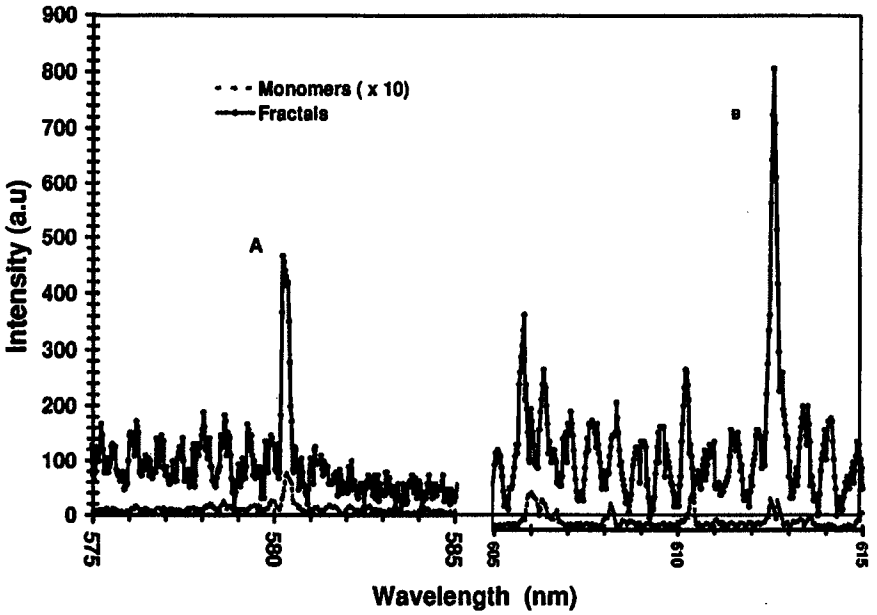

Fig. 9. Inelastic scattering spectra of non-aggregated silver monomers without dye (dashed line, lower trace) and fractal aggregated monomers with 5×10^{-7} M dye solution (solid line, upper trace) in microcavity for $\lambda_L = 543.5$ nm, cw He–Ne laser (maximum power is 0.75 mW).

dependence (see Fig. 9). The threshold power for the 543.5 nm HeNe pump laser was as small as 2×10^{-4} W in these experiments.

The enhanced emission was found to be confined within an approximately 50 μm region of the tube in a vertical direction, which contained the incident pump light; moreover, emission from this region exhibited angular radiation patterns characteristic of microcavity MDR's.

Thus, the spectral, threshold, and spatial dependencies confirm the lasing nature of the observed emission. It is noteworthy that the R6G concentration was only 5×10^{-7} M in these experiments, three orders of magnitude lower than for conventional dye lasers with an external cavity and three orders of magnitude lower than for a microdroplet laser without silver fractal aggregates.[37] These findings suggest that the lasing effect is due to dye molecules adsorbed on the surface of silver aggregates. This conclusion is also supported by the fact that increasing the R6G concentration up to 10^{-5} M did not result in additional growth of the lasing peak intensities over their level for the 5×10^{-7} M dye concentration. The additional dye molecules are apparently not adsorbed onto the silver particles, but remain in solution as free molecules, where they do not effectively contribute to lasing. Lasing emission was observed for R6G concentrations as low as 10^{-8} M, from which we conclude that the surface-enhanced lasing effect was observed for the first time in our experiments.

Microcavity surface-enhanced Raman scattering (SERS) was also investigated. SERS spectra from sodium citrate molecules adsorbed on silver fractal aggregates in a microcavity were obtained under conditions where MDR's either were, or were not, excited (see Figs. 7(a) and 7(b)). We found that SERS is 10^3–10^5 times more intense when MDR's are excited. However, of greater interest is the coupled, multiplicative enhancement factor caused by both fractal aggregates and microcavities. By comparing Raman signal levels from sodium citrate adsorbed on silver colloid aggregates and from a high- molarity sodium citrate solution in the absence of fractal aggregates, we found that SERS enhancement resulting from fractal aggregation of colloidal silver is 10^5–10^6, consistent with the data of Ref. 41. Thus, with the additional, multiplicative, enhancement provided by microcavity MDR's, the resultant average SERS enhancement produced by fractals in a microcavity is estimated to be in the range $10^8 - 10^{11}$. It is also important to note that, since the optical excitations are localized in sub-wavelength, nm-size, regions of the fractal aggregate medium, local enhancement factors can be significantly larger still, up to 10^{16}. These average enhancement factors are comparable with, and can even exceed, the local enhancements for single molecule SERS ($10^{12} - 10^{15}$) observed in Ref. 42. We expect that placing fractal nanostructures in a microcavity will facilitate new possibilities for optical micro-analysis and studies of lasing and nonlinear optical effects in single molecules.

This is illustrated in Fig. 9 which contrasts microcavity spectra of non-aggregated silver monomers without R6G dye (lower trace) with fractal aggregates containing a 5×10^{-7} M dye solution (upper trace) under 543.5 nm HeNe excitation. Two

spectral fragments are shown between 575 and 615 nm. One can see a set of luminescence peaks whose minimal spacing is approximately equal to the intermode spacing of our cylindrical microcavity. In addition, two extremely large peaks distinguish themselves in the observed spectra. We have identified the largest peak (4 times more intense than the emission at 600 nm) at 612.6 nm with the combination Raman band (1310 + 780) cm^{-1} of sodium citrate, used to grow silver monomers, and present in minute (3×10^{-4} M) concentrations in our monomer solutions; the other peak at 580 nm corresponds to the 1160 cm^{-1} fundamental Raman mode of the citrate molecule. These peaks exhibit a nonlinear dependence on pump intensity and may be regarded as surface-enhanced stimulated Raman scattering in a microcavity, excited by a 0.75 mW cw pump laser.

5. Conclusions

This study has shown that forming fractal structures of nanoparticles is an effective way to increase the nonlinear optical response. Localization of plasmon excitations in metal fractal aggregates provides a huge enhancement of local electric fields and, as a result, dramatic increase of the nonlinear susceptibility and figure of merit (FOM). For third-order optical nonlinearity, the FOM as high as 10^{-9} esu $\cdot$ cm was obtained in fractal colloid aggregates at very low metal filling factors $p = 5 \times 10^{-6}$. Nonlinear absorption and refraction coefficients of aggregated colloid solution were found to change signs with wavelength and laser intensity.

The nondegenerate four-wave mixing, characterized by high nonlinear susceptibility $|\chi^{(3)}| > 10^{-7}$ esu, for frequency detuning $|\omega_1 - \omega_2| \leq 28$ cm^{-1} was observed for the nanocomposite of gold imbedded in silica. The response and relaxation time has been determined based on the detuning curve. The $\chi^{(3)}(\omega_3)$ dispersion is governed by different responses with characteristic times of 0.66 ps, 5.3 ps and possibly also by shorter femtosecond time-scale response. The first of the relaxation times was attributed to electron-phonon relaxation, and the second, to thermal diffusion to the host medium.

As a final mechanism for increasing the optical response, composite media, consisting of fractal aggregates seeded into dielectric microcavities, were discussed. Extremely large enhancements of optical emissions are observed in such systems. For example, addition of micromolar concentrations of a laser dye, Rhodamine 6G, to the parent fractal aggregate solution, results in intense lasing emission from the microcavity even for cw pump powers in the sub-mW range.

Acknowledgments

This work was supported in part by NSF under grants DMR-9623663 and DMR-9810183, by Army Research Office (DAAG 55-98-1-0425), Petroleum Research Fund (32319-AC5), NATO, and by RFBR by grant 96-02-19331. J. G. Zhu and N. N. Lepeshkin acknowledge partial support from Los Alamos National Laboratory (New

Mexico Universities Collaborative Research Grant) and Sandia University Research Program, respectively. Oak Ridge National Laboratory is supported by US Department of Energy, under contract DE-AC05-96OR22464 with Lockheed Martin Energy Research Corporation.

References

1. G. L. Fisher, R. W. Boyd, R. J. Gehr, S. A. Jenekhe, J. A. Osaheni, J. E. Sipe and L. A. Weller-Brophy, *Phys. Rev. Lett.* **74**, 1871 (1995); R. J. Gehr, G. L. Fisher, R. W. Boyd and J. E. Sipe, *Phys. Rev.* **B53**, 2792 (1996); R. W. Boyd, R. J. Gehr, G. L. Fisher and J. E. Sipe, *Pure Appl. Opt.* **5**, 505 (1996).
2. Yu. E. Danilova, V. P. Drachev, S. V. Perminov and V. P. Safonov, *Bulletin Russ. Acad. Sci.* **60**, 3, 342 (1996).
3. F. Vallee, N. D. Fatti and C. Flytzanis, in *Nanostructured Materials: Clusters, Composites, and Thin Films*, eds. V. M. Shalaev and M. Moskovits, Chp. 7, p. 70 (American Chemical Society, Washington, DC, 1998); D. Richard, Ph. Roussignol and Chr. Flytzanis, *Opt. Lett.* **10**, 511 (1985).
4. E. J. Heilweil and R. M. Hochstrasser, *J. Chem. Phys.* **82**, 4762 (1985).
5. H. B. Liao, R. F. Xiao, J. S. Fu, P. Yu, G. K. L. Wong and P. Sheng, *Appl. Phys. Lett.* **70**, 1 (1997); H. B. Liao, H. Wang, K. S. Wong and G. K. L. Wong, *Appl. Phys. Lett.* **72**, 1817 (1998); H. B. Liao, R. F. Xiao, J. S. Fu, H. Wang, K. S. Wong and G. K. L. Wong, *Opt. Lett.* **23**, 388 (1998).
6. F. Hache, D. Ricard and C. Flytzanis, *J. Opt. Soc. Am.* **B3**, 1647 (1986); F. Hache, D. Ricard, C. Flytzanis and U. Kreibig, *Appl. Phys.* **A47**, 347 (1988).
7. S. G. Rautian, V. P. Safonov, P. A. Chubakov, V. M. Shalaev and M. I. Stockman, *JETP Lett.* **47**, 243 (1988).
8. K. Uchida, S. Kaneko, S. Omi, C. Hate, H. Tanji, Y. Asahara, A. J. Ikushima, T. Tokizaki and A. Nakamura, *J. Opt. Soc. Am.* **B11**, 1236 (1994).
9. L. Yang, K. Becker, F. M. Smith, R. H. Magruder III, R. F. Haglund, Jr., L. Yang, R. Dorsinville, R. R. Alfano and R. A. Zuhr, *J. Opt. Soc. Am.* **B11**, 457 (1994).
10. Y. Takeda, T. Hioki, T. Motohiro and S. Noda, *Appl. Phys. Lett.* **63**, 3420 (1993).
11. S. G. Rautian, *JETP* **85**, 451 (1997).
12. M. J. Bloemer, J. W. Haus and P. R. Ashley, *J. Opt. Soc. Am.* **B7**, 790 (1990).
13. R. H. Magruder, III, Li Yang, R. F. Haglung Jr., C. W. White, L. Yang, R. Dorsinville and R. R. Altano, *Appl. Phys. Lett.* **62**, 1730 (1993).
14. R. H. M. Groeneveld, R. Sprik and A. Lagendijk, *Phys. Rev.* **B51**, 11433 (1995).
15. C. Suarez, W. E. Bron and T. Juhasz, *Phys. Rev. Lett.* **75**, 4536 (1995).
16. M. Perner, P. Post, U. Lemmer, G. von Plessen, J. Feldmann, U. Becker, M. Mennig, M. Schmitt and H. Schmidt, *Phys. Rev. Lett.* **78**, 2192 (1997); T. Klar, M. Perner, S. Grosse, G. von Plessen, W. Spirkl and J. Feldmann, *Phys. Rev. Lett.* **80**, 4249 (1998).
17. N. Del Fatti, R. Bouffanais, F. Vallee and C. Flytzanis, *Phys. Rev. Lett.* **81**, 922 (1998).
18. J. G. Zhu, C. W. White, J. D. Budai, S. P. Withrow and Y. Chen, *J. Appl. Phys.* **78**, 4386 (1995).
19. A. V. Butenko, P. A. Chubakov, Yu. E. Danilova, S. V. Karpov, A. K. Popov, S. G. Rautian, V. P. Safonov, V. V. Slabko, V. M. Shalaev and M. I. Stockman, *Z. Phys.* **D17**, 283 (1990); V. P. Safonov, V. M. Shalaev, V. A. Markel, Yu. E. Danilova, N. N. Lepeshkin, W. Kim, S. G. Rautian and R. L. Armstrong, *Phys. Rev. Lett.* **80**, 1102 (1998).

20. V. A. Markel, V. M. Shalaev, E. B. Stehel, W. Kim and R. L. Armstrong, *Phys. Rev.* **B53**, 2425 (1996).
21. Yu. E. Danilova, N. N. Lepeshkin, S. G. Rautian and V. P. Safonov, *Physica* **A241**, 231 (1997).
22. A. V. Butenko, V. M. Shalaev and M. I. Stockman, *Z. Phys.* **D10**, 81 (1988).
23. V. A. Markel, L. S. Muratov, M. I. Stockman and T. F. George, *Phys. Rev.* **B43**, 8183 (1991).
24. M. I. Stockman, L. N. Pandey, L. S. Muratov and T. F. George, *Phys. Rev. Lett.* **72**, 2486 (1994).
25. V. M. Shalaev, E. Y. Poliakov and V. A. Markel, *Phys. Rev.* **B53**, 2437 (1996).
26. V. M. Shalaev, *Phys. Rep.* **272**, 61 (1996).
27. J. A. Creighton, C. G. Blatchford and M. G. Albreht, *J. Chem. Soc. Faraday Trans. II* **75**, 790 (1979).
28. P. C. Lee and D. Meisel, *J. Phys. Chem.* **86**, 3391 (1982).
29. V. P. Safonov, J. G. Zhu, N. N. Lepeshkin, R. A. Armstrong, V. M. Shalaev, C. W. White, R. A. Zuhr and Yu. E. Danilova, *Quantum Electr. Laser Science Conf., Technical Digest, QME 5* (Baltimore, 1999).
30. M. Sheik-Bahae, A. A. Said, T. H. Wei, D. J. Hagan and E. W. Van Stryland, *IEEE J. Quantum Electron.* **26**, 760 (1990).
31. V. M. Shalaev, C. Douketis, T. Haslett, T. Stuckless and M. Moskovits, *Phys. Rev.* **B53**, 11193 (1996).
32. C. W. White, D. S. Zhou, J. D. Budai, R. A. Zuhr, R. H. Magruder and D. H. Osborne, *Mat. Res. Soc. Symp. Proc.* **316**, 499 (1994).
33. T. Yajima, *Opt. Commun.* **14**, 378 (1975).
34. G. Frens, *Nature* **241**, 20 (1973).
35. In *Optical Processes in Microcavities*, eds. R. K. Chang and A. J. Campillo (World Scientific, Singapore, 1996); A. Biswas, H. Latifi, R. L. Armstrong and R. G. Pinnick, *Opt. Lett.* **14**, 214 (1988).
36. J. F. Owen, P. W. Barber, P. B. Dorain and R. K. Chang, *Phys. Rev. Lett.* **47**, 1075 (1981).
37. H. M. Tzeng, K. F. Wall, M. B. Long and R. K. Chang, *Opt. Lett.* **9**, 499 (1984).
38. M. B. Lin and A. J. Campillo, *Phys. Rev. Lett.* **73**, 2440 (1994).
39. V. B. Braginsky, M. L. Gorodetsky and V. S. Ilchenko, *Phys. Lett.* **A137**, 393 (1989).
40. W. Kim, V. P. Safonov, V. M. Shalaev and R. L. Armstrong, *Quantum Electr. Laser Science Conf., Technical Digest, QME 4* (Baltimore, 1999).
41. O. Siiman, L. A. Bumm, R. Callaghan, C. G. Blatchford and M. Kerker, *J. Phys. Chem.* **87**, 1014 (1983).
42. K. Kneipp, Y. Yang, H. Kneipp, L. T. Perelman, I. Itzkan, R. R. Dasari and M. S. Feld, *Phys. Rev. Lett.* **78**, 1667 (1997).